Eur. Phys. J. A **19**, 307–317 (2004)
DOI 10.1140/epja/i2003-10126-y

THE EUROPEAN PHYSICAL JOURNAL A

Spectroscopy of ^{40}Ca and negative-parity bands

S. Torilov[1,2], S. Thummerer[2], W. von Oertzen[1,2,a], Tz. Kokalova[1,2], G. de Angelis[2,4], H.G. Bohlen[2], A. Tumino[2,3], M. Axiotis[4], E. Farnea[5], N. Marginean[4], T. Martinez[4], D.R. Napoli[4], M. De Poli[4], S.M. Lenzi[5], C. Ur[5], M. Rousseau[6], and P. Papka[6]

[1] Freie Universität Berlin, Fachbereich Physik, Arnimallee 14, D-14195 Berlin, Germany
[2] Hahn-Meitner-Institut Berlin, Glienicker Strasse 100, D-14109 Berlin, Germany
[3] INFN-Laboratori Nazionali del Sud and Università di Catania, Via S. Sofia 44, I-95123 Catania, Italy
[4] INFN-Laboratori Nazionali di Legnaro, Legnaro, Italy
[5] Dipartimento di Fisica and INFN, Padova, Italy
[6] Institut de Recherches Subatomiques, IReS, Strasbourg, France

Received: 2 May 2003 / Revised version: 23 September 2003 /
Published online: 20 January 2004 –
Communicated by D. Schwalm

Abstract. We have studied the reactions $^{28}\mathrm{Si} + {}^{24}\mathrm{Mg} \rightarrow {}^{52}\mathrm{Fe} \rightarrow {}^{40}\mathrm{Ca}^{*} + 3\alpha$ as well as the binary channel $^{52}\mathrm{Fe} \rightarrow {}^{40}\mathrm{Ca}^{*} + {}^{12}\mathrm{C}^{*}$, in order to search for deformed states, which form rotational bands in ^{40}Ca. We observe positive- and negative-parity bands. The negative-parity band is proposed to be a partner of an inversion doublet with the positive-parity states being based on 4p-4h configurations. The properties of the positive-parity states are discussed on the basis of the shell model and the parity doublet on the basis of a cluster model with intrinsic reflection asymmetric shapes.

PACS. 21.10.-k Properties of nuclei; nuclear energy levels – 21.60.Gx Cluster models

1 Introduction

States in nuclei in the vicinity of the $N = Z$ line are known to show strong clustering phenomena. In particular, several bands in ^{40}Ca have been proposed to have structures, which are based on 4p-4h and 8p-8h excitations [1,2]. Such excitations can also be related to strong α-particle clustering configurations [3–5]. The mentioned states are best populated in reactions in which clustering is already present in the target and the projectile.

A large number of states have been observed in α-particle transfer reactions [3,6–8]. In particular, with the $^{36}\mathrm{Ar}(^{6}\mathrm{Li}, \mathrm{d})$ reaction the spin and parity of many low-lying states have been established [7,8]. The detailed γ-spectroscopy of nuclei around ^{40}Ca has only been recently resumed using highly sensitive γ-detector arrays [9–12]. The most recent result on γ-spectroscopy of ^{40}Ca has established deformed bands with 4p-4h and 8p-8h character [9,13].

To populate ^{40}Ca for γ-spectroscopy we have chosen the $^{24}\mathrm{Mg}(^{28}\mathrm{Si}, 3\alpha)$ reaction at a rather high incident energy of 139 MeV, in order to have the 3α channel with enough counting rate in the compound decay channels. Such incident energy allows the observation of binary reactions with the emission of the $^{12}\mathrm{C}^{*}(0_2^{+})$ state, at an excitation energy of 7.654 MeV, which is at 379 keV above the 3α-threshold in ^{12}C (see also refs. [14]). The Q-value of -7.8 MeV for the three α-particles is the same as for the reaction $^{24}\mathrm{Mg}(^{28}\mathrm{Si}, {}^{12}\mathrm{C}^{*}(0_2^{+}))^{40}\mathrm{Ca}$. The latter can be observed in the silicon ΔE-E detector telescopes by the break-up of this excited state into α-particles.

We report here on the results of the spectroscopy of the ^{40}Ca-nucleus from the $^{24}\mathrm{Mg}(^{28}\mathrm{Si}, 3\alpha)^{40}\mathrm{Ca}$ reaction.

2 Experimental set-up and γ-spectra

The present experiment has been performed with the γ-detector array GASP and the charged-particle detector ball ISIS [15]. In the experiment absorber foils have been used inside the ISIS-ball to prevent the registration of the elastically scattered heavy ions in the silicon detectors. Only light particles up to α-particles were registered.

The detection of heavier (unbound) fragments becomes possible for states with very small decay energies through the decay into α-particles as for $^{8}\mathrm{Be}(0_1^{+})$ and $^{12}\mathrm{C}^{*}(0_2^{+})$. The relevant individual energies of the α-particles in their center-of-mass frame are so small that the decay cone for the two and three α-particles is in the range of 10°–15°, which thus fits well into the opening angle (29°) of one

[a] e-mail: oertzen@hmi.de

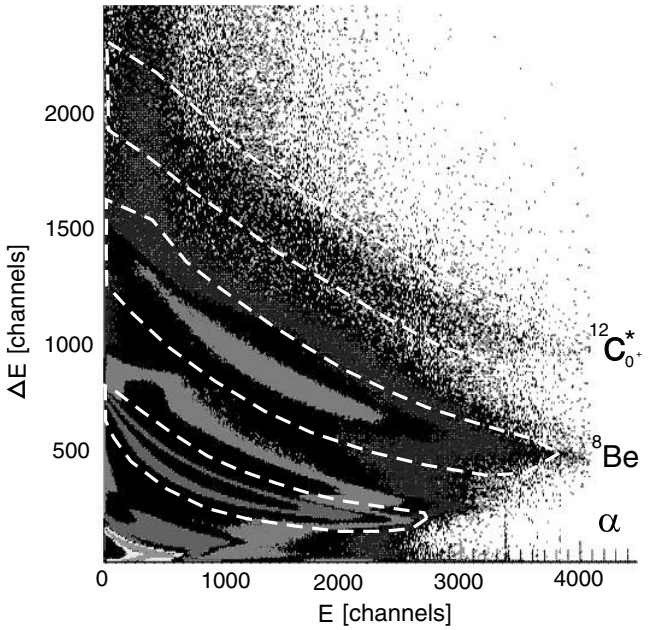

Fig. 1. Plot of ΔE-E signals as observed with the ISIS charged-particle detector system. The events with the emission of single α's, ^{8}Be and with ^{12}C$^{*}(0_2^+)$ are indicated.

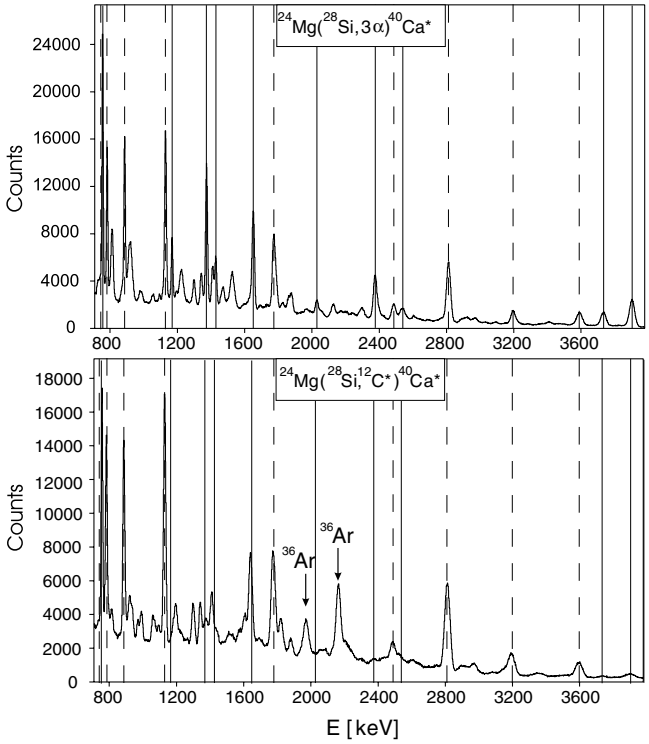

Fig. 2. Doppler-corrected γ-spectrum selected with the 3α channel, and the ^{12}C$^{*}(0_2^+)$ channel, respectively. Solid lines mark the γ-transitions for ^{40}Ca. Dashed lines are the γ-transitions for ^{39}K.

ISIS ΔE-E telescope. Thus, we are able to detect simultaneously the α-particles from the compound decay as well as the spontaneous decay of a weakly bound state by the double and triple pile-up lines. Details on the observation of the ^{8}Be(0_1^+) and the ^{12}C$^{*}(0_2^+)$ are reported in ref. [14] (see also ref. [16]). The ^{24}Mg targets were self-supporting foils of 0.5 mg/cm^2 thickness. At the incident ^{28}Si beam energy of 139 MeV, we have a large contribution of the compound reaction in the 3α channel. We cite the measured total count rates $N(M\alpha)$ for the multiplicities in the 1α up to 4α channels:

$$N(1\alpha) = 8.7 \cdot 10^7,$$
$$N(2\alpha) = 1.5 \cdot 10^7,$$
$$N(3\alpha) = 0.9 \cdot 10^6,$$
$$N(4\alpha) = 0.018 \cdot 10^6.$$

The counts for the binary emission process with ^{12}C* are $0.4 \cdot 10^6$. The relative yields cited correspond to a total geometrical efficiency ϵ of the ISIS-detector ball of ≈ 0.35 for singles (see also ref. [14]). We are able to use both the 3α channel as well as the ^{12}C$^{*}(0_2^+)$ channel for the Doppler-shift correction of the γ-spectra and for the selection of the ^{40}Ca channel; subsequent decays, however, are not selected by this particle trigger, and can only be removed by γ-gating.

2.1 Discussion of the charged-particle and γ-spectra

The relatively high velocity of the compound nucleus and the larger mass emitted mean that the γ-spectra must be corrected for Doppler-shifts on an event-by-event basis. The recoil velocities have been obtained using the momentum vectors of the coincidently registered charged particles. We show in fig. 1 the plot of the charged-particle identification as observed with the ISIS-ball (mainly the first ring with six telescopes contributes in the chosen kinematic conditions). The γ-spectra of ^{40}Ca can thus be obtained with three different charged-particle triggers:

a) 3α-particles,
b) ^{8}Be + α-particle emission, and
c) ^{12}C$^{*}(0_2^+)$ emission.

For all three cases a satisfactory Doppler-shift correction was obtained corresponding, for a 1 MeV γ-transition, to a FWHM of approximately 10 keV.

The energy spectra of the α-particles, the ^{8}Be- and the ^{12}C$^{*}(0_2^+)$ clusters are shown in ref. [14]. We show in fig. 2 the γ-spectra obtained with two different particle gates, the 3α trigger and the ^{12}C$^{*}(0_2^+)$ trigger. In these figures we observe also transitions from other nuclei. After selection of the ^{12}C$^{*}(0_2^+)$ channel we observe a strong increase of ^{39}K as well as of ^{36}Ar transitions (4α-particles emission). The main part next to ^{40}Ca corresponds to ^{39}K, with an additional proton emission. One can see that these peaks are much stronger than those of ^{40}Ca for ^{12}C* emission. One can deduce from the results shown in fig. 2 and fig. 3 that the intensity of the γ-transitions in ^{40}Ca after 3α emission are approximately 12 times larger than after a ^{12}C$^{*}(0_2^+)$ emission.

Further γ-spectra were obtained by setting γ-gates in the higher excitation energy for the establishment of the

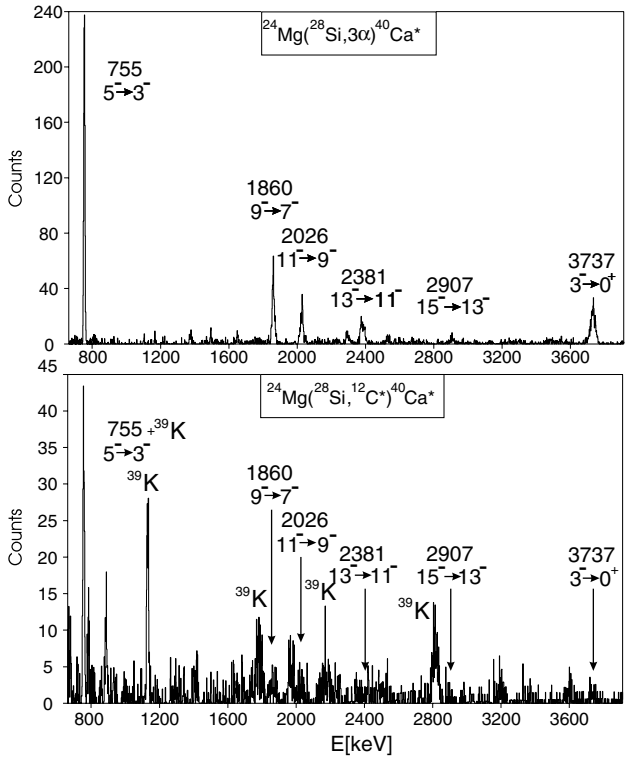

Fig. 3. Doppler-corrected γ-spectrum gated by the 4542 keV ($7^- \rightarrow 5^-$) transition (see fig. 5) in ^{40}Ca, and selected with the 3α and the ^{12}C*(0_2^+) channels, respectively.

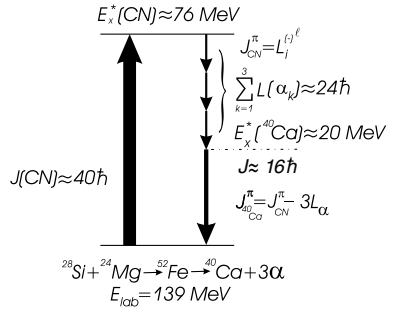

Fig. 4. Energy to angular-momentum relations for the average compound emission of 3α-particles. The average J-value of the compound nucleus is $40\hbar$.

decay scheme shown later (fig. 5 in sect. 3.1). For example, the gate on the 4542 keV led to the "negative-parity band" shown in fig. 3. In the gating procedure we have energy regions which are severely hindered by the presence of γ-decays in ^{39}K, a fact which influences the usefulness of the DCO values (see below).

An important feature of the chosen reaction channels is the possible selectivity to states with natural parity in the residual nucleus. The compound nucleus is populated by spin zero in the projectile and the target, forming only natural-parity states, with parity $\pi = (-)^J$ for spin J, where $L(= J)$ is the relative angular momentum in the incident channel. If only α-particles with spin zero are emitted at the entry line for γ-decay, the states in the residual nucleus will have natural parity. This statement will also hold if the subsequent statistical γ-rays down to the first near yrast γ-lines will be predominantly of $E1$-character, which are, however, suppressed in $N = Z$ ($T = 0$) nuclei. Statistical $M1$-transitions are also possible, but with a reduced probability (typically by a factor 10 or more for $T = 0$ nuclei due to their isovector character) and unnatural parities could appear (some states in ref. [9] are assigned as unnatural parity).

If the 3α-particle decay populates directly the yrast states at the highest excitation energies a natural-parity band will be populated. At variance with this observation are the *non-yrast states* on the right-hand side of fig. 5, which tentatively are assigned as unnatural-parity states (in analogy to states observed in ^{44}Ti). Their population is very weak, a fact which would be expected because they are not directly populated via 3α emission, but by γ-decay.

The *energetics of the energy angular-momentum balance* are illustrated in fig. 4. For the calculation of the angular momentum of the outgoing α-particles, we used the standard equation

$$L_b^{\max} = R_b \frac{\sqrt{2m_b(E_b - V_b)}}{\hbar}\,.$$

Here R_b is the interaction radius for the emitted particle from the residual nucleus (with a parameter for the radii, $r_0 = 1.5$ fm), E_b is the energy in the center-of-mass system, V_b is the Coulomb barrier and m_b the reduced mass of the emitted particle. The compound nucleus is populated with an average value of $L_{\rm CN} = 40\hbar$, see fig. 4. For the single α-particles, the most probable energy carried away is 18–20 MeV (see ref. [17]), and we obtain average values of the angular momenta of $L_\alpha \approx 8\hbar$. The highest-lying states in ^{40}Ca reached in the 3α emission, which populate the observed γ-decay path, are thus located at $J \approx 16^+$ and at $E^* \approx 20$ MeV (see fig. 4), and for the present reaction they should have natural parity.

Due to the energetics of the reaction the three α-particle emission can be regarded to be energetically stretched, leaving little freedom for statistical γ-decays before the first γ-decay of a rotational band is observed. In ref. [14] we actually show that in the present experiment the observed chance triple-hit probability in the ^{12}C* branch is extremely small as compared to the expected value for a statistical emission, deduced from the single hits. This fact indicates that in the α-particle emission the three steps of the emission are *not* statistically independent, and this may explain the special population of the negative-parity states.

3 Spectroscopic results for ^{40}Ca

From gating on different transitions, a level scheme has been established, which contains the main transitions already observed in refs. [9,13]. We also observe the deformed band denoted as 8p-8h by Ideguchi *et al.* [9], with the first observed level at 5630 MeV. In our case with a detector set-up of smaller efficiency, the observed population

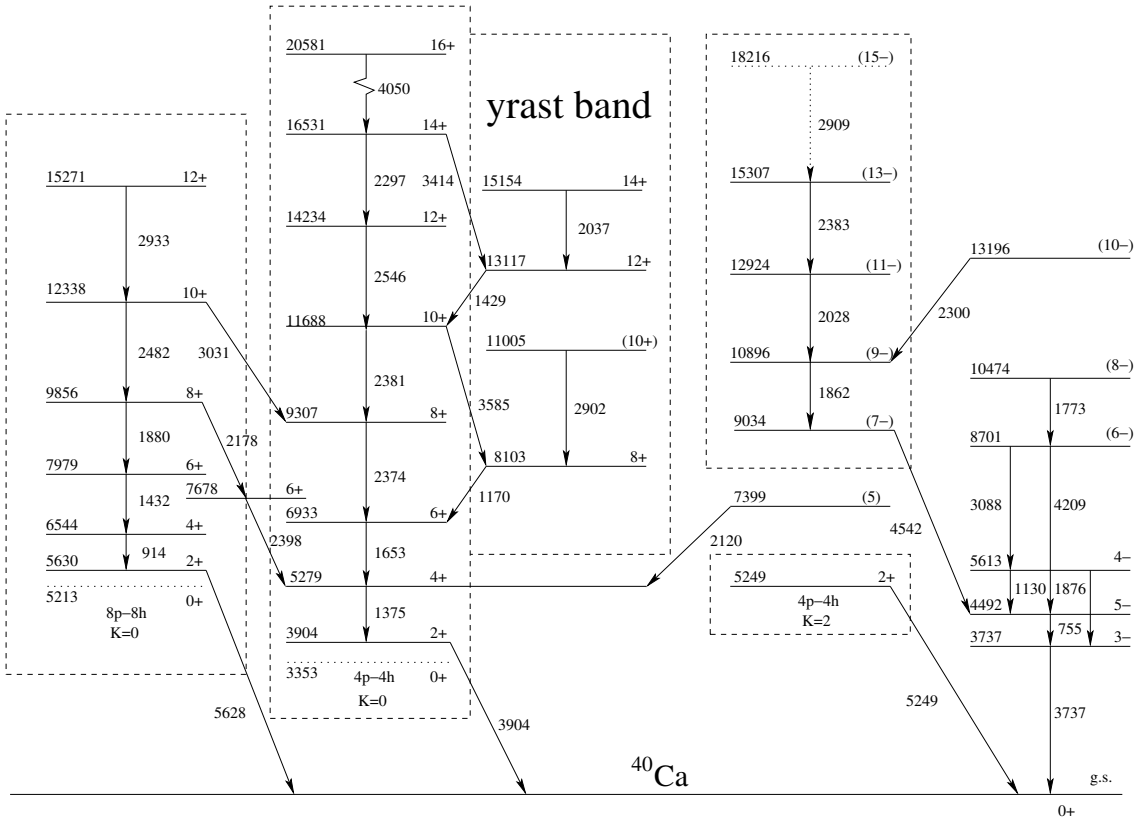

Fig. 5. Level scheme of ^{40}Ca as obtained in the present experiment. The states are grouped into bands of positive parity (4p-4h, $K = 0$, $K = 2$), (8p-8h), and a negative-parity band and some remaining transitions.

ends at a spin of 12. In contrast to ref. [9], we observe further additional transitions corresponding to states at 9034, 10896, 12924 and 15307 keV. These are states, which can be attributed to a band with negative parity. As explained in the previous section, due to the properties of the reaction with 3α emission we expect in ^{40}Ca mainly the direct population (and subsequent decays) of states with natural parity. These states decay via strong $E2$-transitions also into negative-parity states, which finally decay into the well-known states (of shell model structures) with spin parity of 3^- and 5^- (see fig. 5).

In ref. [9] three transitions are cited to have characteristics of dipole ($E1$ or $M1$) transitions:

a) The 2120 keV transition from the state at 7399 keV; we suggest that this state is a member of our negative-parity band, thus it may have spin parity assigment 5^- and the transition seems to be $E1$. We do not observe the feeding transition to this state.
b) A transition with 2004 keV, not observed in our case.
c) A transition with 2037 keV; this transition appears in ref. [9] as a transition between the 13^+ state (at 15154 keV) and the 12^+ (at 13117 keV) state.

The assignments of states for the proposed negative-parity band in our case relies strongly on previous work of the ^{36}Ar(^{6}Li, d) reaction and they are partially established through the determination of the DCO values which are cited in table 1. In this table the intensities of the γ-transitions for the $R_{\rm DCO}$ ratio are also shown.

Table 1. Energies of γ-transitions, DCO values (with the errors) for intensities gated by the 4542 keV ($E2$) transition and proposed multipolarities.

E (keV)	$I_{\rm DCO}$ I	$I_{\rm DCO}$ II	$R_{\rm DCO}$	Proposed multipolarity
755	45(7)	46(7)	1.0(0.2)	$E2$, calibr.
1862	18(5)	15(5)	1.2(0.4)	$E2$
2028	7(3)	16(7)	0.4(0.3)	($E2$), see text
2383	11(4)	9(3)	1.2(0.6)	$E2$
3737	22(5)	15(4)	1.5(0.5)	$E3$

As shown in ref. [18] the ratio $R_{\rm DCO}$,

$$R_{\rm DCO} = \frac{I_{\gamma 1}(\theta_1) \text{ gated by } \gamma_2(\theta_2)}{I_{\gamma 1}(\theta_2) \text{ gated by } \gamma_2(\theta_1)},$$

can be used to determine multipolarities. For the gate the transition with 4542 keV was used which is well resolved and narrow; for the angles we took 34° *versus* 90° for the value of the numerator and 90° *versus* 146° for the denominator's value. For the calibration of the the DCO values for certain multipolarities we start with the well-known transitions 755 keV ($5^- \rightarrow 3^-(E2)$) and 3737 keV ($3^- \rightarrow 0^+(E3)$) [19]. According to this data, we determine the other DCO values shown in table 1. Some of the DCO

Table 2. Proposed negative-parity bands in ^{40}Ca and in ^{44}Ti; they are proposed to be the partners of the 4p-4h band, and of the 4p-0h band, respectively, see table 3 and fig. 6. Δ_γ shows the proposed or observed energy of the γ-transitions.

J^π (^{40}Ca) proposed	E^* (MeV)	Popul.	Δ_γ (MeV)	Comments refs.
1^-	5.902	(^{6}Li, d)		[6]
3^-	6.58/6.28	(^{6}Li, d)	0.68/0.38	[6]
5^-	7.399	(γ-γ)	0.82/1.12	present work
7^-	9.034	(p, p′)	1.635	[20]
9^-	10.896	(γ-γ)	1.862	present work
11^-	12.924	(γ-γ)	2.028	present work
13^-	15.307	(γ-γ)	2.383	present work
15^-	18.216	(γ-γ)	2.909	present work
J^π (^{44}Ti)	E^* (MeV)	Popul.	Δ_γ (MeV)	Comments refs.
3^-	3.174	(γ-γ)		[21]
5^-	4.059	(γ-γ)	0.884	”
7^-	5.661	(γ-γ)	1.602	”
9^-	7.397	(γ-γ)	1.736	”
11^-	9.711	(γ-γ)	2.314	”

values are at the limit of the statistical significance and the spin and parity assingments have been put into parentheses. A serious problem arises also due to background due to γ-transitions in ^{39}K, whose energies coincide with transitions in ^{40}Ca and the occurrence of energy doublets in transition energies in ^{40}Ca.

The listed DCO values (table 1) are all compatible with $E2$-character (or $E3$ as indicated), except for the transition with 2028 keV contaminated by ^{39}K, where we have $R_{\rm DCO}$ smaller than unity. This energy is close to a strong $M1(E2)$ transition of 2061 keV between two $11/2^-$ states in ^{39}K. The 755 keV transition is strong in our case, therefore the 757 keV transition in ^{39}K is not so relevant. For the 1862 keV transition in ^{40}Ca we have a coincidence in energy with a low-lying transition in ^{39}K with 1864 keV, however, with smaller influence on the result.

The energy sequence and the intensity flux pattern allow us to establish for a number of the subsequent higher-lying states that they belong to the same band and we suggest negative parity.

The decay scheme of the present experiment shown in fig. 5 thus differs from the previously reported level/decay scheme [9] due to the presence of a negative-parity band. Further, there are the unnatural-parity states in ref. [9], the state at 7399 is attributed as 5^+, and the state at 15154 is 13^+.

In our analysis the fit to the energies of the γ-transitions gave values systematically 2 keV lower than those observed by Ideguchi *et al.* [9]. This uncertainty easily occurs due to different fitting procedures of the peaks. We adopt the values of ref. [9] and therefore the energies of the transitions in fig. 5 have been increased by 2 keV as compared to the values given in fig. 3, in order to better comply with the observed decay scheme of ref. [9]. We observe one transition from the “5^-” state

Table 3. Comparison of the the positive-parity bands in ^{40}Ca, ^{36}Ar and ^{44}Ti, corresponding to structures with (4p-4h), (4p-8h) and (4p-0h), respectively; they are the proposed partners of the negative-parity bands observed in ^{40}Ca and ^{44}Ti, respectively, shown in fig. 6 and listed in table 2.

J^π $K=0^+$	E^*	Popul.	Δ_γ	Comments
^{40}Ca	(MeV)		(MeV)	refs.
0^+	3.353	(^{6}Li, d)		[6]
2^+	3.904	(^{6}Li, d)	0.511	[6]
4^+	5.279	(^{6}Li, d)	1.375	[6]
6^+	6.933	(^{6}Li, d)	1.653	[6]
8^+	9.307	(γ-γ)	2.374	[9], pres. work
10^+	11.688	(γ-γ)	2.381	“
12^+	14.234	(γ-γ)	2.546	“
14^+	16.531	(γ-γ)	2.297	“
16^+	20.581	(γ-γ)	4.050	“
^{36}Ar	(MeV)			ref. [10]/Γ
0^+	4.329			$\leq$4 keV
2^+	4.951	(γ-γ)	0.622	$\leq$ 35 keV
4^+	6.137	(γ-γ)	1.186	$\leq$ 35 keV
6^+	7.767	(γ-γ)	1.630	57 keV
8^+	9.927	(γ-γ)	2.160	120 keV
10^+	12.748	(γ-γ)	2.821	
12^+	15.350	(γ-γ)	2.602	
14^+	18.298	(γ-γ)	2.948	
16^+	22.362	(γ-γ)	4.064	
^{44}Ti	(MeV)			
0^+	0.0			[21]
2^+	1.083	(γ-γ)		
4^+	2.454	(γ-γ)	1.371	”
6^+	4.015	(γ-γ)	1.561	”
8^+	6.508	(γ-γ)	2.493	”
10^+	7.670	(γ-γ)	1.162	band terminating

(at 7399 MeV) to the 4^+ state (at 5279 MeV), which is consistent with an $E1$-transition; in ref. [9], however, $M1$ is assumed. This state had no visible feeding transition in our data, it is most likely fed from the 6^- state at 8701 MeV (with 1322 MeV, this energy is very close to a contaminant line of ^{39}K), at variance with ref. [9], but the decay pattern proposed here is completely analogous to that observed in ^{44}Ti (see ref. [21]). Also in this work a side-feeding into the negative-parity band is observed, in our case from the (10^-) state to the (9^-) state with $E_\gamma = 2300$ keV. However, the transitions from $(8^-, 6^-)$ to $(7^-, 5^-)$ with 1440 keV and 1302 keV are very weak, because the main decay goes via $E2$, they can only be separated in our spectra from the very strong ^{39}K-lines (both not marked in fig. 3).

The fact that $E1$-transitions are present points to the non-negligible isospin mixing observed in these $N = Z$ nuclei, see ref. [22].

In an approach with an intrinsically reflection asymmetric (octupole) deformation [3,23,24] we expect a parity doublet for the 4p-4h configuration in ^{40}Ca. For the

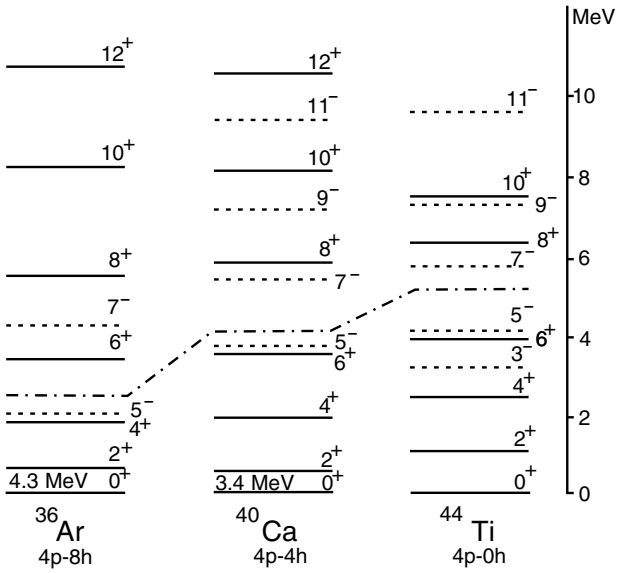

Fig. 6. Energy level schemes for nuclei with the 4p-Xh structure, where X is 8, 4, or 0. The dashed lines correspond to the negative-parity partners for the cited bands of positive parity. The dashed-dotted line is the α-threshold. In ^{44}Ti, the band has its termination point at $J = 12\hbar$. For ^{44}Ti, the band head with 0^+ corresponds to the ground state, for ^{40}Ca to a state at 3353 keV and in ^{36}Ar to a state at 4329 keV excitation energy.

discussion it is useful to compare our findings for the negative-parity bands, as far as they are established in the neighbouring $N = Z$ nuclei, namely in ^{36}Ar and ^{44}Ti. We list in table 2 and table 3 the states corresponding to the proposed parity doublets (the 4p-Xh bands and their partners). The comparison is illustrated in fig. 6. We find indeed a similar structure in these nuclei.

3.1 The states of the proposed parity doublet

In the following we will concentrate on the negative-parity states in ^{40}Ca. Negative-parity states were previously identified mostly via the ^{36}Ar(^{6}Li, d) reaction. In order to get a tentative correspondence with the previous work, we list in the following the members of the proposed parity doublet (first the negative-parity states).

We first discuss some of the low-lying states of negative parity, which are well described by the shell model (2^-, 3^-, 4^-, 5^-).

3.1.1 3.737 MeV, 3^-

This is the first-excited state (with non-zero angular momentum) in ^{40}Ca. From the shell model point of view, this state corresponds to a 1p-1h $(d_{3/2})^{-1}(f_{7/2})^1$ configuration and has the correct spin and energy position as predicted in different shell model calculations [25].

3.1.2 4.492 MeV, 5^-

This is the second state of the 1p-1h structure. It was observed as a strong peak in the inelastic scattering of α-particles on ^{40}Ca by [26]. According to the shell model, this is the last state of the $(d_{3/2})^{-1}(f_{7/2})^1$ configuration. In the present experiment, there is only one strong transition to this level. The other transitions (right part of the level scheme for the negative-parity states) are very weak and only two of the γ-transitions (1130 keV and 1876 keV) have been observed before.

3.1.3 The proposed K = 0^- band

We proceed to discuss the states proposed to form a negative-parity band ($K = 0^-$) with the assumption that it is the partner of the 4p-4h band. A band with $K \neq 0$ would appear independently for a strongly clustered state with a core of fixed deformed geometry, which is not spherically symmetric, namely with an instrinsic structure (like a triangle or a "flower", see ref. [27]).

3.1.4 5.902 MeV, 1^-

Although this state is not observed in the present decay pattern, we start tentatively with a 1^- state. It was observed in the reaction (^{6}Li,d) as a weak peak [6]. Because the minimum spin for the configuration $(d_{3/2})^{-1}(f_{7/2})^1$ corresponds to 2^-, it seems that this 1^- level can be used to start a band with a mixture of configurations like 3p-3h and 5p-5h. This level was not observed in the present study, because we have more intensity in the decay from the higher-spin state of this band to the 1p-1h shell model states (see below). Usually, for the negative-parity bands we expect a transition like $3^-_1 \rightarrow 2^+_1$ (in ^{36}Ar,^{44}Ti), but in the case of ^{40}Ca, the 3^-_1 is the first-excited state, and no transition of this type can exist.

3.1.5 6.28 MeV, 3^-_2, 6.58 MeV, 3^-_3

As candidates for the second state of the band we have two 3^- states. Both of these states were observed in (^{6}Li, d) reactions [6,7] as very weak peaks. Both are not observed in the present experiment.

3.1.6 7.399 MeV, (5^-_2)

The next 5^- state after the 1p-1h states is not observed in γ-decay studies, nor in the α-transfer reactions. If our approach with rotational properties of previous levels is right, this level should have an energy position near 7–7.5 MeV. Other states are observed in the reactions (^{6}Li, d) and (α-α') [3,26], the candidates appear as very weak peaks at 7.11 MeV, 7.47 MeV and 7.57 MeV. As in ref. [9], we observe a dipole transition to the 4^+ state, there this state is assigned as (5^+). We thus cannot be sure about its parity; however, from the comparison with the systematics shown in fig. 6, we suggest that a 5^- should be expected at this energy.

3.1.7 9.034 MeV, (7^-)

This is the first state of the proposed rotational band which is observed in the present experiment. This level was observed in reactions like (p, p') [20] and (p, γ) [28]. According to the first reference, this state has spin 5^-, the second one gives 4^-. From comparison with the neighbouring nuclei ^{36}Ar and ^{44}Ti, we marked this level as 7^-. The same conclusion we get from the DCO ratio. The γ-transition with an energy of 4.542 MeV goes to the 5_1^- state at 4.492 MeV. This transition corresponds to the strongest γ-peak in the spectrum of negative-parity states for the levels with excitation energies larger than 4.5 MeV. The spectrum gated on this peak is shown in fig. 3. In the gate of 4542 KeV we cannot see the transition of this rotational band from the 7^- state to the 5_2^- state (1635 keV) (see the previous section). In other gates, it is very very weak (there appears a possible line in the 3737 keV gate), the main reason being the strong $E2$ transition with $E_\gamma = 4542$ keV to 5_1^-, with a 120 times larger probability than the same kind of transition with an energy around 1600 keV to the 5_2^- at 7.399 MeV (slightly counterbalanced by a smaller $B(E)$ value and the efficiency difference). In ref. [9] this state is not observed.

3.1.8 10.896 MeV, (9^-)

From this level there is only one transition to the 9.034 MeV level as shown in fig. 3. According to this spectrum, the sum of transition intensities feeding into this level is approximately equal to the intensity outgoing with the 1.862 MeV transition.

3.1.9 12.924 MeV, (11^-)

We have two candidates for the next member of the rotational band with two transitions feeding into the 9^- level. Because the transition from the 13.196 MeV level is approximately a factor two weaker than the transition from this level, we can conclude that the proposed state is a member of the negative-parity rotational band.

3.1.10 15.307 MeV, (13^-)

This is the last well-observed state of this band. According to fig. 3, its transition energy is 2383 keV and the subsequent 2028 keV transition has approximately the same intensity, thus confirming our assumption.

3.1.11 18.216 MeV, (15^-)

There is one very weak peak (more than three times weaker than the other transitions of the band) which we see in the spectra (upper part of fig. 5) gated for different transitions. Because this state is very close to the limit of maximal excitation energy (approximately 20 MeV) of the residual ^{40}Ca nucleus, we assume that it has natural parity and that we can see no more transitions, even if this band has no termination on this point.

3.1.12 The $K = 0_2^+$ band (4p-4h)

The corresponding 4p-4h band would consist of the following members.

3.1.13 3.353 MeV, 0_2^+

This is the second 0_2^+ state, and was not observed in the present experiment. According to the model calculations of ref. [1], this state is described as strongly deformed with the major configuration involving the promotion of four particles from the *sd* to the *fp* shell (4p-4h). This state is considered to be the starting point of the rotational band with well-known members at 3.9 MeV, 2^+ and at 5.28 MeV, 4^+ [6,26,29].

3.1.14 6.933 MeV, 6^+

This state was observed in the ^{28}Si(^{14}N, pnγ)^{40}Ca reaction [30]. This is the last level of the rotational band with 4p-4h structure, which is a member of the yrast line. After this level we observe a strong splitting of the 4p-4h band into the "left" and "right" side parts shown in fig. 5. According to ref. [27], for this particle-hole structure there are two shapes corresponding to oblate and prolate deformations, these two bands exhibit configuration mixing.

The 6^+ level at 6.93 MeV and the level 8^+ at 8.1 MeV were observed in ref. [30], the latter is the first level of the "right-side" part of the 4p-4h rotational band in fig. 5. There are two transitions to this level: 3585 keV (this is a very weak connection between the opposite-side bands) and 2902 keV. The second transition starts from the 11.005 MeV level (probably spin 10) which is a member of the right-side band. In ref. [9] the last observed level of this band is at 15.154 MeV and is assigned as spin 13^+, because of the multipolarity of the 2037 keV transition. The remaining states of this band are well observed with transitions up to the 16^+ state. In our case with the 3α emission for near yrast states the population of only natural parity is possible.

3.1.15 $K = 0_3^+$ band (8p-8h)

The other group of known states from ref. [9,13] is also observed in the present work, it corresponds to the 8p-8h band with 5.21 MeV for the 0^+ state, 5.63 MeV for the 2^+ and 6.54 MeV for the 4^+ [6]. After these there follow very weak transitions with 1432 keV (the level 7.979 MeV, 6^+) and 1880 keV. The next known excited states of this band were observed by Braun-Munzinger [31] with slightly different excitation energies in the reaction ^{36}Ar(^{16}O,^{12}C)^{40}Ca. These are the states at 12.4 MeV, 10^+ and at 9.9 MeV, 8^+. The transition between these two levels is much stronger than the other transition down to this level because at this point there is a connection between the 8p-8h band and the 4p-4h band (through the level 6^+ at 7.678 MeV). The last state with spin 12^+ at 15.271 MeV is not populated in low-energy ^{36}Ar(^{6}Li, d) reactions and is observed only in ref. [9] and in the present work.

Table 4. Moments of inertia for $K = 0^+$ and $K = 0^-$ rotational bands in nuclei around ^{40}Ca. For the calculation of the rotational constant for the di-nuclear system the expression for the moment of inertia from ref. [32] was used, and the relative distance between the clusters is, *e.g.*, $R_m = R_\alpha + R_{\rm Ar}$.

Nucleus	Band head	α (keV)	Ref.
^{36}Ar	0_2^+	65	[12]
^{40}Ca	$0_2^+/0_3^+/7^-$	62/64/49	[9], present work
^{42}Ca	0_2^+	62	[33,34]
^{44}Ti	$0_2^+/3^-$	62/55	[21]
dinucl. syst. (^{36}Ar + α)		81	[32]

3.2 Summary of the evidence for parity doublets

As a conclusion from the reported decay scheme and the survey of the literature, we try to identify the inversion doublet partners of the deformed bands based on cluster structure with an α-particle and ^{36}Ar core. Further we can try to relate these structures to rotational bands of similar character in neighbouring nuclei, namely to multi-particle multi-hole excitations, like the 4p-8h configurations in ^{36}Ar and 4p-0h, in ^{44}Ti, see fig. 6. Indeed, we observe negative-parity states with the same character, 5^-, 7^-, in the vicinity of the thresholds in all these nuclei.

The main structure of the parity doublets must thus be related to intrinsic reflection asymmetric (octupole) shapes due to octupole shapes or clustering. The latter dominates in light nuclei, whereas stable octupole deformation occurs in heavy deformed nuclei on the basis of the mixing of particular shell model orbits. The level structures observed in ^{36}Ar [27] and ^{44}Ti are shown in fig. 6, where the corresponding knowledge on the possible parity doublets in the neighbouring $N = Z$ nuclei is compiled. In all cases, the 5^- states are observed just below the α-particle thresholds, which are indicated by the dash-dotted line.

We compare the moments of inertia for the three cases of fig. 6 in table 4. The estimate of the rotational constant α ($\alpha = \frac{\hbar^2}{2\theta}$), was obtained from fitting the experimental data for the energy levels by

$$E(J) = \alpha[J(J+1)]\,.$$

As shown in ref. [32], the moment of inertia of the di-nuclear systems can be described by the expression

$$\theta = \theta_1 + \theta_2 + m_0 \frac{A_1 A_2}{A} R_m^2\,.$$

Here, θ_i are the rigid-body moments of inertia for the nuclei constituting the di-nuclear system, A_i and $A = (A_1 + A_2)$ are mass numbers, m_0 is the nucleon mass and R_m is the distance between the center of the clusters.

The proposed bands have large moments of inertia, with values of α near 60 keV. This value is very close to the prediction of moments of inertia (α) for shape-isomers for heavy nuclei. With the (A)-dependence of $\alpha(A) = 30985$ keV$/A^{5/3}$ of ref. [35] and $R_x = 0.96\ A^{1/3}$, we have $\alpha(40) = 66.2$ keV for ^{40}Ca in good agreement with the value in table 4. The main rotational bands proposed in this work are later summarized in fig. 8. The second band with 4p-4h character mixes with the first one. The energy splitting of the proposed inversion doublet tends to zero for higher spins.

Fig. 7. Schematic illustration of the two inverted shapes of the inversion doublet in ^{40}Ca, consisting of an ^{36}Ar + α structure.

4 Discussion and conclusions

Parity doublets as rotational bands have been observed in atomic nuclei in many mass regions of the nuclear chart [24,36]. The occurrence of the octupole shapes finally mentioned in the shell model picture is attributed to mixing of Nilsson orbits with angular momenta differing by 3 units. Thus the feature of stable pear-shaped nuclei is a feature well described by the shell model. In contrast, octupole shapes in light nuclei are observed as a consequence of intrinsic reflection asymmetric shapes due to clustering [3,24]. We expect a transition region between these two extremes for the mass 40 nuclei, namely a coexistence of the shell model features and the cluster description of octupole deformations [37,38], and the observations reported here can be understood as an indication of the change from cluster and shell model approaches. Octupole shapes are also predicted in ^{40}Ca from Cranked Hartree-Fock calculations [39], where the softness to β_3 deformations is obtained as a function of quadrupole deformation.

The relevant structure has no intrinsic parity, the observable states are produced by spin and parity projection as shown in fig. 7, and the positive- and negative-parity states are obtained. However, if the larger cluster has no spherical shape, an independent band with negative parity may appear due to a fixed intrinsic geometry and an unusual sequence of spins (*e.g.*, 5^-, 6^-, 7^-) could result.

The general feature of octupole shapes in these nuclei is the observation of a doublet of negative- and positive-parity bands. These two bands should have the following properties:

I) The moments of inertia of the two bands are almost the same.
II) The bands start in their excitation energy close to the separation energy thresholds for α-particles.
III) The two bands have only a relatively small difference in their excitation energies, namely the energy splitting ΔE, if compared on a common $J(J+1)$ scale (as an example, see fig. 8) is small. The splitting, however, depends on the properties of the barrier between the two configurations and vanishes at higher angular momentum.

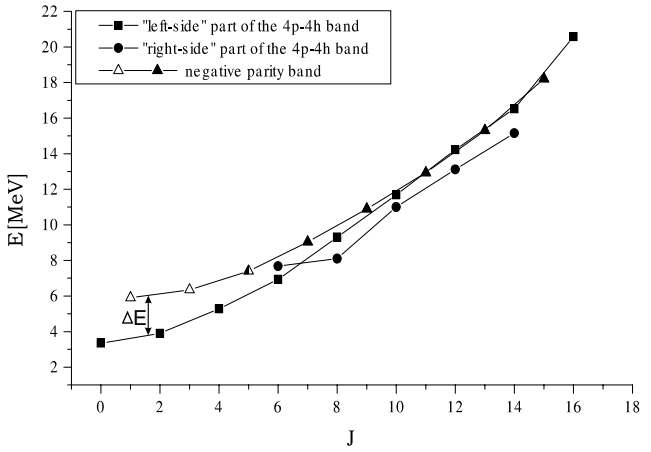

Fig. 8. Plot of the proposed rotational bands in ^{40}Ca with different parities. Open triangles correspond to the levels, which were not observed in the present experiment. The half-solid triangle is the 5^- state.

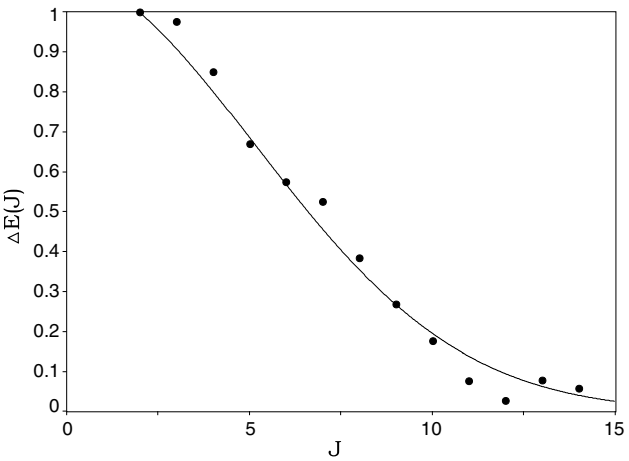

Fig. 9. Dependence of the energy splitting ΔE as a function of J of the two partners of an inversion doublet of the 3.353 MeV (0_2^+) 4p-4h band in ^{40}Ca. The curve is calculated according to the approach of Jolos *et al.* [36,40]. For the states of negative parity, the values of the energies from table 2 were used.

IV) The energies of the states of these bands show good agreement with a $J(J+1)$-dependence. This, however, is well fulfilled only in heavier nuclei, where configuration mixing is less important.

Examples for comparison with our results are the molecular states with asymmetric cluster structure in ^{16}O and ^{20}Ne; these cases have rather clear features of cluster states (see also refs. [3,37]). In heavier nuclei, like the actinides [23,24,36] we have rather pure deformed shell model configurations within the levels of a band.

From the shell model point of view, we can consider the excited states of ^{40}Ca as n-particles–n-hole states. There are two positive-parity bands in this nucleus (4p-4h, 8p-8h). For the 4p-4h band, a negative-parity band as an inversion partner has been identified in the work of [3]; these are the negative-parity states *above the α-particle threshold*, which are *very strongly* populated in ^{36}Ar(^{6}Li, d) reactions. In the present work, we include states in the new band, which are weakly populated in the mentioned reaction and the higher-lying observed states are usually weakly populated in α-transfer (also because of the angular-momentum barrier).

With the observation of the proposed negative-parity band we suggest the possible existence of another inversion doublet partner based on mixed cluster and shell model configurations. Actually, the positive-parity states in ^{40}Ca are described in the shell model framework, but will be mixed with the ^{36}Ar + α structure as proposed by Ohkubo [37]. For the negative-parity structure we have two possibilities, our band based on 3p-3h excitations in the shell model configurations, which can mix with cluster configurations, but also with low-lying 1p-1h states. The other is the high-lying negative-parity band of Ohkubo (starting with 1^- at 8.15 MeV); this band exhibits indeed a very large energy splitting characteristic of a cluster model, and the states have large α-width.

We will try to obtain the energy splitting ΔE between the presently proposed band partners by using the model of Jolos *et al.* [36,40]; it is obtained by an interpolation like

$$\Delta E = \langle \Psi^- H \Psi^- \rangle - \langle \Psi^+ H \Psi^+ \rangle \,.$$

In fig. 8 we show the bands proposed in this work plotted as a function of spin J, and we observe the diminishing energy splitting. The model by Jolos and von Brentano [36,40], predicts the spin (energy) dependence of the splitting $\Delta E(J)$ for the two octupole bands using the picture of a double well in the octupole degree of freedom with an inner barrier. The result applied to our data is illustrated in fig. 9.

The comparison of the bands with opposite parity and the behavior of the splitting, as a function of angular moment is done by considering the tunneling transitions between the two octupole shapes. Here we have used the normalized parity splitting $\Delta E(J)$:

$$\Delta E(J) \equiv \overline{\Delta E(J)} / \overline{\Delta E(2)} \,.$$

Here $\overline{\Delta E(J)}$ is defined as

$$\overline{\Delta E(J)} = \frac{1}{2} | E(J) - 2E(J-1) - \frac{1}{4} [E(J+2) - 2E(J) + E(J-2)] | \,.$$

According to the tunneling model of refs. [40,36], the values for the splitting $\Delta E(J)$ are calculated as (the factor a parametrizes changes in the moments of inertia with J and I as parameters)

$$\Delta E(J) = \exp \left[- \frac{J(J+1)/I(I+1)}{1 + aJ(J+1)} + \frac{6/I(I+1)}{1+6a} \right] .$$

The observation of an energy splitting in the inversion doublet implies a certain probability to switch between

Table 5. The values of the splitting energy $\delta E(J)$ with $J = 3\hbar$ for different nuclei showing parity split bands.

Nucleus	δE (MeV)	Reference
^{16}O	2.96	[3]
^{20}Ne	4.22	[3]
^{40}Ca	1.81	present work
^{40}Ca (theor.)	5.51	[3]
^{40}Ca (theor.)	1.54	[41]
^{44}Ti	1.41	[21]

the two inversion shapes shown in fig. 7. As predicted in ref. [40], the parity splitting of the states decreases exponentially with $J(J+1)$; the comparison to our data is shown in fig. 9. Actually, the curves are not as smooth as in the case of heavy nuclei, where pure (shell model) bands of rotational character are observed. We also observe, see fig. 8, that the 4p-4h band has a strong deviation from the $J(J+1)$ rule, and that two bands are crossing approximately at spin $11\hbar$. Still we observe a fairly good agreement with the model of refs. [36,40], the splitting tends to zero for higher spin values, as predicted.

We compare the values of the observed energy splitting for bands with octupole deformation in different nuclei; for this we use a value of $J = 3$ in the equation

$$\delta E(J) = E(J)^- - \frac{1}{2}(E(J+1)^+ + E(J-1)^+)\,.$$

The results of this calculation for different cases are given in table 5.

The energy splitting and the energy position of the states with negative parity of the present case (^{40}Ca) has actually been predicted by Jolos [41], independently of our experimental results on the basis of the energies of the 4p-4h positive-parity band.

Finally, we resume the discussion of our result in the light of the predictions for negative-parity bands in ^{40}Ca by Ohkubo [3,37]. This work based on the cluster model places the purely cluster band of negative parity at a much higher energy (above the α-particle threshold), and a corresponding large energy splitting is obtained (see table 5). The different configurations and excitation modes contributing to the states of given spin and parity are actually discussed (and shown in tables in ref. [37]) on the basis of the orthogonality condition model (OCM), which allows the simultaneous description of simpler shell model configurations and the cluster model states. There, predictions for the low-lying negative-parity states (*e.g.*, 1^- and 3^-) are also made; they show a strong splitting in strength and a mixing of configurations with shell model character. These features explain their γ-decay into shell model states, and their smaller (α)-width. The structure of the states calculated in the frame of the OCM model thus supports the observation of two negative-parity bands: i) a mixed cluster-shell-model–based (3p-3h) band suggested in this work and, ii) a cluster-model–based band at a higher excitation energy. We may thus conclude that the mass-40 region exhibits octupole deformation with a transitional character between pure cluster structures (like ^{20}Ne) and pear-shaped deformed shell model configurations observed in heavier nuclei.

This work was supported by the BMBF grant Nr. 06-OB-900. Tz. Kokalova thanks the DAAD for their grant. We also thank the A.v. Humboldt foundation for support (A. Tumino and G. de Angelis). We acknowledge very fruitful discussions with R.V. Jolos, and we thank S. Ohkubo and the referee for their important comments to this work.

References

1. W.J. Gerace, A.M. Green, Nucl. Phys. A **93**, 110 (1967).
2. W.J. Gerace, A.M. Green, Nucl. Phys. A **123**, 241 (1969).
3. S. Ohkubo *et al.*, Prog. Theor. Phys. Suppl. **132**, 1 (1998).
4. K. Ikeda, N. Tagikawa, H. Horiuchi, Prog. Theor. Phys. (Jpn.) Extra Vol. Suppl. **64** (1968).
5. G. Reidemeister, S. Ohkubo, F. Michel., Phys. Rev. C **41**, 63 (1990).
6. H.T. Fortune *et al.*, Phys. Rev. C **19**, 756 (1979).
7. T. Yamaya *et al.*, Nucl. Phys. A **573**, 154 (1994).
8. T. Yamaya *et al.*, Phys. Rev. C **53**, 131 (1996).
9. E. Ideguchi *et al.*, Phys. Rev. Lett. **87**, 222501 (2001).
10. C.S. Svensson *et al.*, Physics Division Annual Report, Argonne National Laboratory ANL-00/20, c63 (1999).
11. D. Rudolph *et al.*, Phys. Rev. C **65**, 03430 (2000).
12. C.S. Svensson *et al.*, Phys. Rev. C **63**, 061301 (2001).
13. J.C. Chiara, E. Ideguchi, M. Devlin *et al.*, Phys. Rev. **67**, 041303R (2003).
14. Tz. Kokalova, Thesis, FU Berlin July 2003, to be published.
15. D. Bazzacco, *Proceedings of the International Conference on Nuclear Structure at High Angular Momentum, (Ottawa, 1992)* Vol. **2**, Report No. AECL 10613 (AECL Research, Ottawa, 1992) p. 376.
16. S. Thummerer *et al.*, J. Phys. G **27**, 1405 (2001).
17. H. Morgenstern *et al.*, Z. Phys. A **313**, 39 (1983).
18. K.S. Krane, R.M. Steffen, R.M. Wheeler, Nucl. Data Tables **11**, 351 (1973).
19. P.M. Endt, Nucl. Phys. A **521**, 1 (1990).
20. C.R. Gruhn *et al.*, Phys. Rev. C **6**, 915 (1972).
21. C.D. O'Leary *et al.*, Phys. Rev. C **61**, 064314 (2000).
22. E. Farnea *et al.*, Phys. Lett. B **551**, 56 (2003).
23. H. Horiuchi, K. Ikeda, Prog. Theor. Phys. **40**, 277 (1968).
24. P.A. Butler, W. Nazarewicz, Rev. Mod. Phys. **68**, 350 (1996).
25. W.J. Gerace, A.M. Green, Nucl. Phys. A **113**, 641 (1968).
26. E.P. Lippincott, A.M. Bernstein, Phys. Rev. **163**, 1170 (1967).
27. Y. Kanada-En'yo *et al.*, arXiv:nucl-th/0208078 v1 30Aug2002.
28. S.W. Kikstra *et al.*, Nucl. Phys. A **512**, 425 (1990).
29. R. Middleton *et al.*, Phys. Lett. B **39**, 339 (1972).
30. J.J. Simpson *et al.*, Phys. Rev. Lett. **35**, 23 (1975).
31. P. Braun-Munzinger *et al.*, Phys. Rev. Lett. **29**, 1261 (1972).
32. T.M. Shneidman *et al.*, Nucl. Phys. A **671**, 119 (2000).
33. S. Torilov, Thesis 2003, St. Petersbirg University.
34. M. Lach *et al.*, Eur. Phys. J. A **16**, 309 (2003).
35. H. Schultheis, R. Schultheis, Phys. Rev. C **27**, 1367 (1983).

36. T.M. Shneidman *et al.*, Phys. Rev. C **67**, 014313 (2003).
37. T. Sakuda, S. Ohkubo, Prog. Theor. Phys. Suppl. **132**, 103 (1998).
38. S. Ohkubo, private communication.
39. T. Inakura *et al.*, Nucl. Phys. A **710**, 261 (2002).
40. R.V. Jolos, P. von Brentano, Phys. Rev. C **49**, R2301 (1994).
41. R.V. Jolos, private communication.